Formation of manganese δ-doped atomic layer in wurtzite GaN

Meng Shi, Abhijit Chinchore, Kangkang Wang, Andrada-Oana Mandru, Yinghao Liu et al.

Citation: J. Appl. Phys. **112**, 053517 (2012); doi: 10.1063/1.4750034
View online: http://dx.doi.org/10.1063/1.4750034
View Table of Contents: http://jap.aip.org/resource/1/JAPIAU/v112/i5
Published by the American Institute of Physics.

Formation of manganese δ-doped atomic layer in wurtzite GaN

Meng Shi, Abhijit Chinchore, Kangkang Wang, Andrada-Oana Mandru, Yinghao Liu, and Arthur R. Smith[a)]

Department of Physics and Astronomy, Nanoscale and Quantum Phenomena Institute, Ohio University, Athens, Ohio 45701, USA

(Received 19 December 2011; accepted 9 August 2012; published online 7 September 2012)

We describe the formation of a δ-doped manganese layer embedded within *c*-plane wurtzite gallium nitride using a special molecular beam epitaxy growth process. Manganese is first deposited on the gallium-poor GaN $(000\bar{1})$ surface, forming a $\sqrt{3}\times\sqrt{3}-R30^\circ$ reconstructed phase. This well-defined surface reconstruction is then nitrided using plasma nitridation, and gallium nitride is overgrown. The manganese content of the $\sqrt{3}\times\sqrt{3}-R30^\circ$ phase, namely one Mn per each $\sqrt{3}\times\sqrt{3}-R30^\circ$ unit cell, implies that the MnGaN alloy layer has a Mn concentration of up to 33%. The structure and chemical content of the surface are monitored beginning from the initial growth stage up through the overgrowth of 20 additional monolayers (MLs) of GaN. An exponential-like drop-off of the Mn signal with increasing GaN monolayers, as measured by Auger electron spectroscopy, indicates that the highly concentrated Mn layer remains at the δ-doped interface. A model of the resultant δ-doped structure is formulated based on the experimental data, and implications for possible spintronic applications are discussed. © *2012 American Institute of Physics*. [http://dx.doi.org/10.1063/1.4750034]

I. INTRODUCTION

The importance of spintronics in general was emphatically described by Wolf *et al.*,[1] while the possibility to fabricate room-temperature spintronic devices based on GaN was proposed by Dietl *et al.*[2] The idea, based on a mean-field Zener model calculation, was to create a dilute magnetic semiconductor (DMS) involving GaN doped with a few percent Mn, and it was predicted to be ferromagnetic (FM) at or above room temperature. Moreover, GaN-based spintronic DMS systems are particularly attractive for spin-injection applications, as it has been predicted that the spin lifetime in GaN is 3 orders of magnitude larger than that in GaAs.[3] More recently, first principles calculations have been applied by many different researchers in order to determine the magnetic and electronic states induced by doping GaN with various transition metal impurities.[4–7]

Experimentally, manganese doping of GaN has been well studied, with many interesting results having been reported very early.[8–11] The incorporation of Mn in Ga-polar GaN is complicated to some extent because of the Ga bi-layer, which plays an important role in normal GaN growth. This metallic Ga bi-layer also impacts the growth of MnGaN, making the Mn incorporation a strong function of the growth conditions as they range between N-rich and Ga-rich.[12,13] In particular, the Mn incorporation was found to drop off precipitously with increasing Ga-rich conditions. Furthermore, there have been indications of $GaMn_3N$ clusters precipitating under stoichiometric conditions for Mn concentrations more than a couple of percent.[13] To try to avoid this type of problem and alongside the developing effort studying Mn-doping of GaN, many other semiconducting host materials have been investigated including silicon, germanium, gallium phosphide, silicon carbide, and zinc oxide just to name a few, in order to realize a room temperature DMS material without second-phase precipitation.[14–21] In addition, many different dopant species, both transition metal and rare earth, have also been tried.[22–24] To date however, the search continues for the ideal DMS system.

Very recently, Cui *et al.* have investigated δ-doping of GaN/AlN heterostructures theoretically as a potentially attractive alternative to bulk DMS doping, in order to achieve more effective spin injection properties.[25,26] Conceptually, this involves laying down just a single layer of dopants and then overgrowing with bulk material, thus achieving a highly concentrated dopant layer, hopefully without the dopants having had time to form second-phase precipitates. A digital δ-doped layer offers the possibility to achieve a high concentration of dopants. Cui *et al.* calculated based on first-principles in fact that for 1/4 monolayer (ML) and 1/2 ML, the doped layer (either Mn or Cr) becomes FM half-metallic (HM), while for a complete 1 ML coverage (Mn or Cr), it becomes FM (spin-polarization up to 69%) but metallic. This is then particularly attractive, since with the 100% spin polarization achieved in a HM system, coupled with the intrinsic ability of DMS systems to overcome the so-called conductivity mismatch problem, it may be possible to realize 100% efficient spin injection in a realistic GaN-based DMS system. The challenge then is to experimentally realize such a digital δ-doped system in GaN.

In this paper, we present an experimental study of digital δ-doping in wurtzite GaN. To avoid the Mn incorporation problem due to the Ga bi-layer on the Ga-polar face, we choose the N-polar $(000\bar{1})$ face and make use of an intrinsic Mn-induced $\sqrt{3}\times\sqrt{3}-R30^\circ$ reconstruction, in order to populate the GaN surface with a high concentration of Mn dopants.[27] The $\sqrt{3}\times\sqrt{3}-R30^\circ$ reconstruction plays the role of a template for the Mn dopants, thus opening the

[a)]e-mail: smitha2@ohio.edu.

possibility that the dopants will be prevented from interacting with each other, thereby avoiding the formation of Mn-rich precipitates. Nitridation and subsequent GaN overgrowth of the Mn dopant layer is carried out, and structural and chemical measurements are presented which address the question regarding how effectively this method results in a high concentration of Mn dopants remaining at the interface. In this way, we address the suitability of digital δ-doping as a means to potentially produce a spintronic material system in wurtzite GaN.

II. EXPERIMENTAL METHOD AND PROCEDURE

The experiments are performed in a molecular beam epitaxy (MBE) chamber equipped with reflection high energy electron diffraction (RHEED) for monitoring the evolution of the surface during growth and processing. The sample may be transferred directly into an adjoining ultra-high vacuum (UHV) surface analysis chamber containing scanning tunneling microscopy (STM) and Auger electron spectroscopy (AES) capabilities. The system is depicted in Fig. 1.

Growth of GaN on sapphire is accomplished by using a Ga effusion cell and an rf N-plasma nitrogen source. During growth, the sample is mounted on a sample stage, which may be heated up to 1000 °C. The RHEED electron beam has energy of 20.0 keV, and the pattern is collected onto a phosphor screen and imaged using a CCD camera, which displays the pattern on a computer screen as well as allowing electronic data capture.

The substrates used are (0001)-oriented sapphire having size of 1.0 cm × 1.0 cm; substrates are coated by Ti on the backside to absorb the heat radiation from the heater. Substrates are typically cleaned in acetone and isopropanol before being loaded into the MBE chamber. The process of the initial GaN growth and annealing, Mn deposition and processing, and further overgrowth of GaN is depicted in Fig. 2.

Once inside the MBE chamber, the substrate is heated up to ∼1000 °C and simultaneously nitrided for up to 30 min. Following this step, the substrate is lowered to the buffer layer growth temperature (∼600 °C) with plasma running, and then the Ga cell is opened at a flux which is known to produce smooth GaN growth (typically $1-3\times10^{14}$ atoms/cm^2/s).

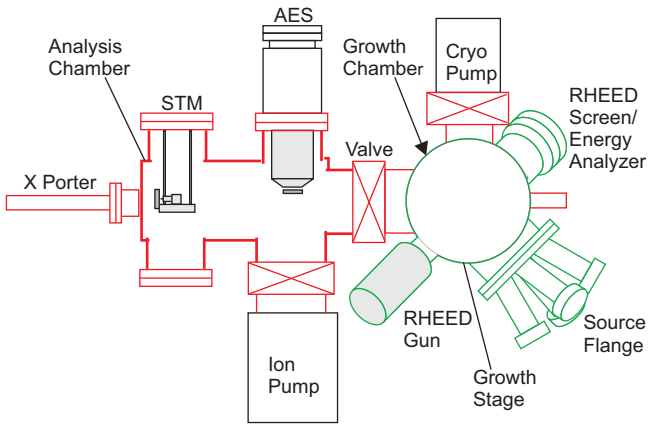

FIG. 1. Diagram of the experimental system.

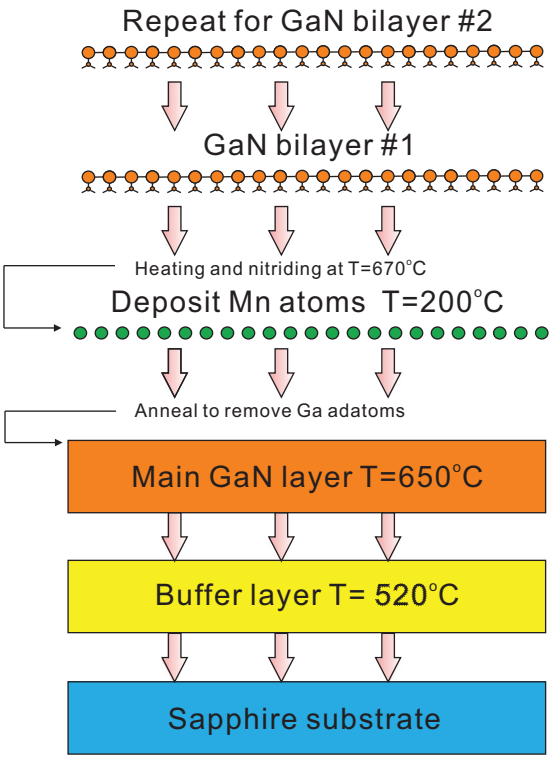

FIG. 2. Schematic diagram of the GaN growth, Mn deposition, and subsequent GaN overgrowth process.

After a short period of buffer growth (∼5 min), the substrate is heated to a higher temperature (∼700 °C) for the main GaN layer growth. The main GaN layer growth time is ∼1 h or more. This growth procedure results in N-polar GaN.

Following the successful smooth growth of GaN as judged by streaky RHEED patterns along both [11$\bar{2}$0] and [10$\bar{1}$0], the GaN sample is cooled to ∼200 °C. If higher order reconstruction lines are seen such as 3rd order diffraction streaks, the sample is annealed to within the range 700–750 °C in order to remove Ga adatoms and Ga droplets. Finally, a RHEED pattern showing mainly 1 × 1 is obtained at low temperatures (∼200 °C or less).

Synthesis of the Mn-containing layer proceeds with the sample held at ∼200 °C and by deposition of a small quantity of Mn by means of a Mn effusion cell. In this experiment, the amount of Mn evaporated is ∼2/3 ML, where a ML of Mn is defined in terms of the density of Ga on the GaN surface (so, 1 ML = 1.135×10^{15}/cm^2). After deposition, 1/3rd and 2/3rd order streaks appear clearly along [10$\bar{1}$0], indicative of a $\sqrt{3}\times\sqrt{3}-R30^\circ$ reconstruction. The actual Mn content of the $\sqrt{3}\times\sqrt{3}-R30^\circ$ can be estimated by AES (see Sec. III). Deposition at temperatures higher than 200 °C also leads to the $\sqrt{3}\times\sqrt{3}-R30^\circ$ structure but at a reduced sticking rate. If the Mn coverage is reduced, this would presumably lead to localized patches without Mn and localized patches of $\sqrt{3}\times\sqrt{3}-R30^\circ$ with Mn.

The $\sqrt{3}\times\sqrt{3}-R30^\circ$ phase is then the starting point for the subsequent formation of the δ-doped layer. This begins by exposing the $\sqrt{3}\times\sqrt{3}-R30^\circ$ structure to nitrogen and nitrogen plasma and heating to the GaN growth temperature. The nitridation process is explored by RHEED and

by AES. Following the nitridation of the $\sqrt{3} \times \sqrt{3} - R30°$ structure, and with the N plasma still active, GaN is overgrown by simply opening the Ga shutter and restarting MBE growth of GaN.

Different experiments are carried out, including monitoring the nitridation and GaN overgrowth process by RHEED in a continuous fashion using the SCAN mode of the RHEED system to acquire a continuous movie evolution of the RHEED pattern and RHEED streak spacing. This is done for both the $[10\bar{1}0]$ and $[11\bar{2}0]$ azimuths. In addition, start-and-stop type growth and analysis experiments are carried out, in which the GaN growth is interrupted after successive MLs of GaN are overgrown, in order to measure the Mn, Ga, and N signals by AES as a function of overgrowth thickness.

The accumulated information is then analyzed by careful measurements of RHEED streak spacings as functions of the nitridation and overgrowth time, and the AES snapshot information is used to determine the rate at which the Mn signal drops off with GaN overgrowth.

Finally, x-ray diffraction (XRD) is carried out in order to measure the *c* lattice constant.

III. RESULTS AND DISCUSSION

A. GaN growth and surface structure

Presented in Fig. 3 is RHEED and STM data corresponding to the initial growth of the GaN layer on sapphire(0001). Shown in Fig. 3(a) is the RHEED pattern for the GaN surface just after growth at the growth temperature where a $1\times$ pattern is observed. This is typical for GaN growth under Ga-rich conditions. After cooling down to less than $\sim$300 °C, as shown in Fig. 3(b), the pattern shows $\frac{1}{3}$

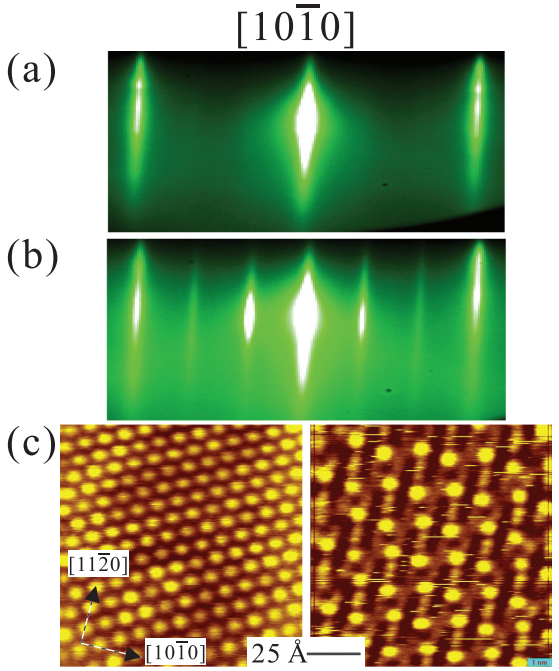

FIG. 3. RHEED and STM of GaN$(000\bar{1})$ surface grown by MBE. (a) RHEED of GaN surface at the growth temperature; (b) RHEED after cooling to room temperature; (c) STM images of GaN$(000\bar{1})$ showing 3×3 reconstruction (left) and $c(6 \times 12)$ reconstruction (right).

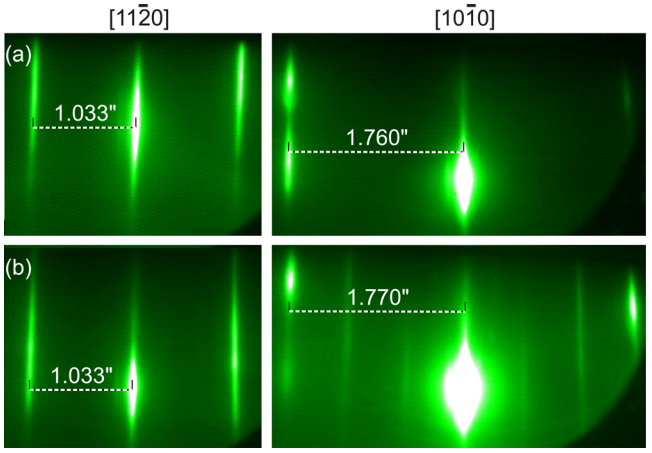

FIG. 4. RHEED images (a) before and (b) after Mn deposition along both $(11\bar{2}0)$ and $(10\bar{1}0)$, as indicated.

order streaks, indicating a $3\times$ periodicity. This is seen along both azimuths—$[11\bar{2}0]$ and $[10\bar{1}0]$. This pattern has been shown to correspond to the 3×3 Ga adatom-on-adlayer reconstruction, which was first understood in 1997.[28]

Displayed in Fig. 3(c) are STM images of the resulting GaN surface acquired at room temperature. The image on the left is of the 3×3 reconstruction in which Ga adatoms occupy every 3rd site along the high symmetry directions, whereas the image on the right is of the $c(6 \times 12)$ reconstruction, which has a slightly more complicated model.[29] Both of these structures contain Ga adatoms; the 3×3 model contains 1/9th ML of Ga adatoms. In Ref. 29, the $c(6 \times 12)$ is modeled to contain 2/9th ML of Ga adatoms. For the next step of this project, we anneal the sample with the goal to remove these adatoms and create a 1×1 surface structure.

Annealing of the as-grown GaN$(000\bar{1})$ surface results in removal of Ga adatoms and Ga droplets from the surface and ultimately 1×1 RHEED patterns are obtained as shown in Fig. 4(a). There we see that the 1/3rd- and 2/3-order streaks are removed, indicating that the surface has very little remaining Ga adatoms and that the surface is mostly in a 1×1 surface structure. After careful calibration of our RHEED system, we also discovered that the *in-plane* lattice constant after annealing is expanded isotropically relative to bulk stoichiometric values by as much as 5%. We show in the next sections that this expansion may be attributed to a fractional loss of N from the sample which occurred during annealing.

B. Deposition of manganese and composition measurement

Manganese is deposited onto the 1×1 GaN$(000\bar{1})$ surface, and the RHEED pattern changes distinctly as shown in Fig. 4(b). Along $[10\bar{1}0]$, the pattern develops distinct $\frac{1}{3}$ and $\frac{2}{3}$ order streaks, whereas along $[11\bar{2}0]$, the pattern remains in a 1×1 state. These RHEED patterns correspond to a $\sqrt{3} \times \sqrt{3} - R30°$ unit cell.[27] The integral streak spacing of the $\sqrt{3} \times \sqrt{3} - R30°$ pattern is measured and compared with that of the surface prior to Mn deposition; it is found that there is no change in streak spacing during Mn deposition along either azimuth to within 0.6%.

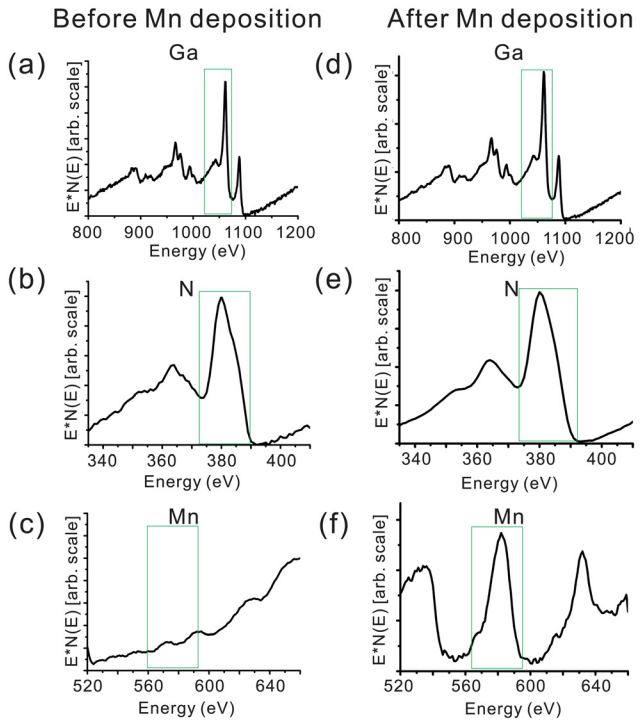

FIG. 5. AES spectra (integrated) of GaN$(000\bar{1})$ surface before and after Mn deposition: (a)–(c) are Ga, N, and Mn AES spectral regions (1064 eV, 380 eV, and 582 eV, respectively) before Mn deposition; (d)–(f) are Ga, N, and Mn AES spectral regions after Mn deposition. Green boxes indicate the peaks of interest.

To determine the chemical content of the surfaces corresponding to the RHEED patterns shown in Figs. 4(a) and 4(b), AES was performed, as shown in Fig. 5. Figures 5(a)–5(c) are the AES spectra before Mn deposition, corresponding with Ga, N, and Mn spectral regions, respectively. Figures 5(d)–5(f) are the corresponding spectra after Mn deposition, for comparison. While Ga and N AES peaks are clearly seen in Figs. 5(a)–5(e), no Mn signal is found prior to Mn deposition, as shown in Fig. 5(c), whereas after Mn deposition, Mn is clearly observed, as shown in Fig. 5(f).

From these spectra, derivative spectra were calculated in order to perform composition analysis using known AES sensitivity factors, which are relevant to derivative spectra. From the resulting amplitudes of the primary AES derivative peaks for Ga, N, and Mn, the elemental ratios Ga:N, Mn:N, and Mn:Ga were calculated. The results after Mn deposition show that Ga:N = 1.15; Mn:N = 0.11; and Mn:Ga = 0.10. Although in principle, Ga = N at the surface, the terminating layer should be a Ga layer (Ga adlayer); therefore the calculated Ga : N > 1 is reasonable. At the same time, since the AES elemental ratios are sensitive to several complete bilayers of Ga and N, but only to one partial surface layer of Mn, the surface Mn coverage (in MLs) would be significantly larger than the elemental AES ratio calculated.

Supposing Ga and N peaks correspond effectively to m contributing layers of GaN, the surface Mn coverage in MLs should be: $\theta_{Mn} \cong \text{Mn} : \text{N} \times m$ (in MLs), where we assume that N remains constant after Mn deposition. Assuming $m \sim 3$–4, we get that $\theta_{Mn} \cong 0.3$–0.4 ML. This is consistent with the amount of Mn, which would be contained within a $\sqrt{3} \times \sqrt{3} - R30^\circ$ structure having 1 Mn per unit cell (= 0.33 ML); it is also consistent with the amount of Mn deposited (2/3rd ML) × the sticking coefficient at 200 °C (~ 0.4) = 0.3 ML. This surface corresponds to the starting point for subsequent processing steps including annealing, nitridation, and finally growth of additional MLs of GaN, which shall be discussed in the following sections.

C. Effect of annealing and nitridation

As can be seen in the RHEED pattern of Fig. 6(a), heating the Mn-covered surface to as high as 670 °C does not destroy the $\sqrt{3} \times \sqrt{3} - R30^\circ$ structure. Still, the $\frac{1}{3}$ and $\frac{2}{3}$ order streaks can be observed. This means that the $\sqrt{3} \times \sqrt{3} - R30^\circ$ structure is quite stable. Heating to yet higher temperatures (e.g., more than 700 °C), finally results in loss of the fractional order Mn-induced streaks, but in addition the GaN surface itself begins to dissociate.

Despite the stability of the $\sqrt{3} \times \sqrt{3} - R30^\circ$ with temperature, exposure of the surface to N_2 at room temperature results in disappearance of the fractional ordering streaks. This is seen clearly in Fig. 6(b). After the N_2 exposure, the sample was again measured by AES, with the result for the Mn peak displayed in Fig. 6(c). The Mn peak is not reduced in intensity, thus showing that Mn atoms are not removed from the surface by the N_2 exposure. This result suggests that

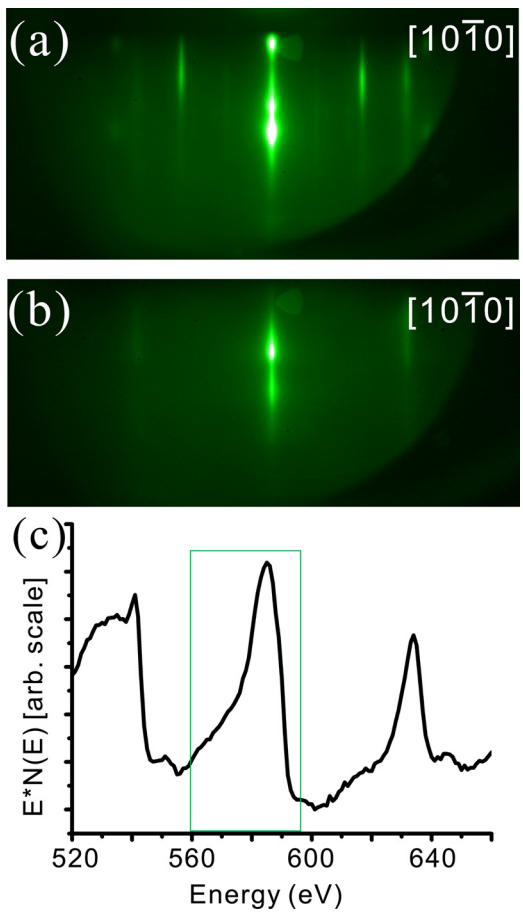

FIG. 6. (a) RHEED image after annealing to high temperature. (b) RHEED image after nitridation. (c) Mn AES spectrum showing Mn 582 eV peak after nitridation.

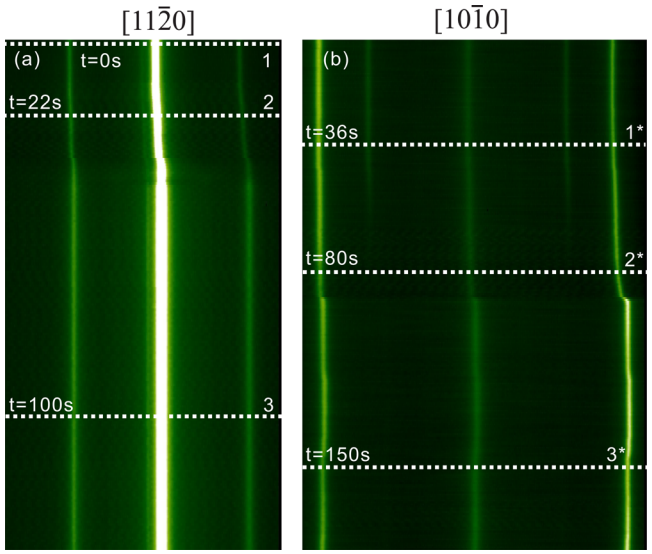

FIG. 7. (a) RHEED scan-mode image along (11$\bar{2}$0). Line 1: t = 0 s, open nitrogen gas into chamber. Line 2: t = 22 s, plasma on. Line 3: t = 100 s, plasma off. (b) RHEED scan-mode image along (10$\bar{1}$0). Line 1*: t = 36 s, open nitrogen gas into chamber. Line 2*: t = 80 s, plasma on. Line 3*: t = 150 s, plasma off.

the Mn-containing (cation) layer is covered over with a N (anion) layer, and thus the reconstruction streaks disappear.

We find that the exposure of the surface to nitrogen plasma also results in the reversion of the *in-plane* lattice constant back to a GaN bulk-like stoichiometric value ($a = 3.189$ Å). The RHEED patterns along [11$\bar{2}$0] and [10$\bar{1}$0] are recorded in scan mode as a function of time, as presented in Figs. 7(a) and 7(b), respectively. The scan mode images along both azimuths show the changing of the streak spacings as well as some lateral shifts, which commonly occur during activation of the plasma source. Also, along [10$\bar{1}$0], the fading out of the 2/3rd-order streaks is clearly seen as the surface is being nitridated.

From the scan mode data, the streak spacing is carefully measured starting from before exposing the surface to N_2 gas, until after the plasma is lit and running and finally turned off. As can be seen in Figs. 8(a) and 8(c), the RHEED streak spacing between the 1× streaks increases rapidly along both azimuthal directions, corresponding to a bi-axial lattice contraction in real space [Figs. 8(b) and 8(d)]. By calibration, we find that this contracted value corresponds to a GaN bulk-like stoichiometric lattice constant.

It can be noticed that the increase in streak spacing with time is not precisely linear. This can be understood, since it takes some time for the plasma source to be lit (done manually). As such, along [11$\bar{2}$0] for example, at t = 0 s, N_2 gas is opened into chamber, RHEED streak spacing starts to increase. A small shoulder appears after ~22 s indicating a partial lattice contraction. At that point, the plasma source is turned on and gradually activated. Then at t = 32 s, after a total ~3.6% change, the lattice constant has regained its

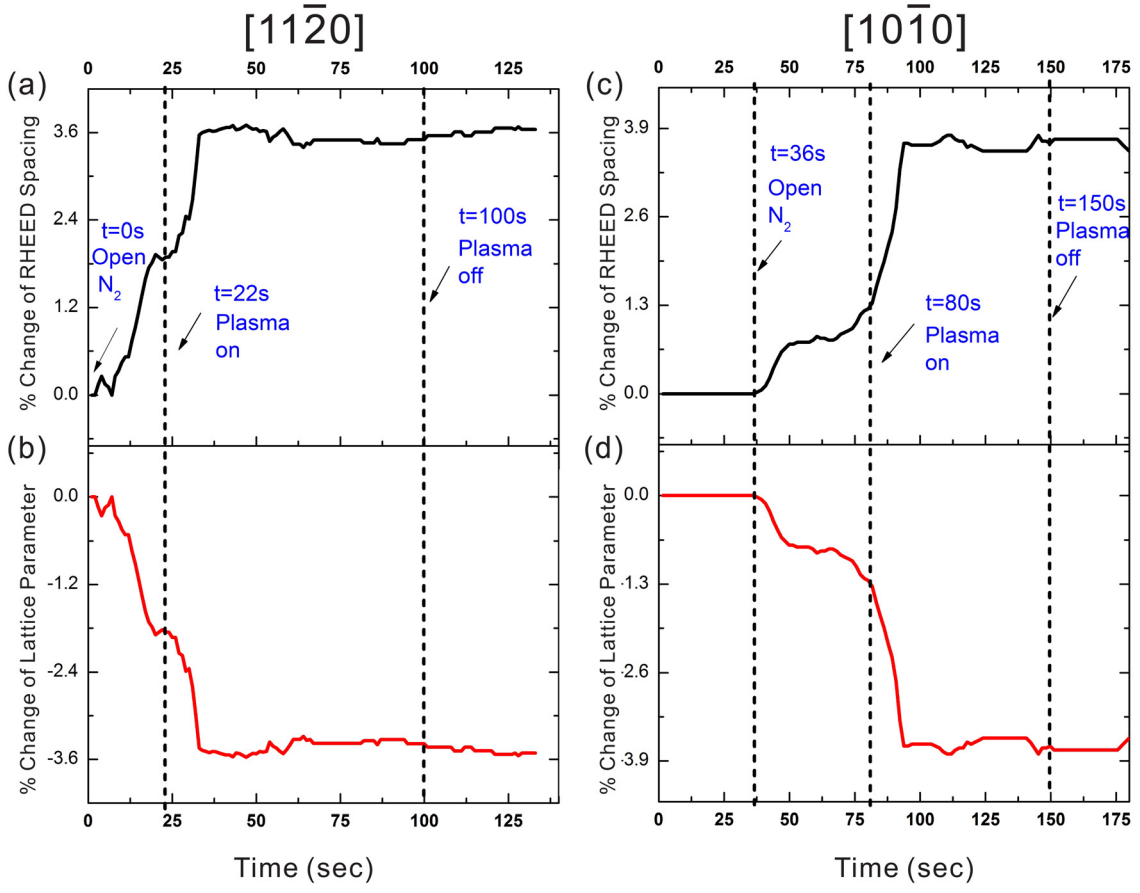

FIG. 8. % changes in RHEED streak spacings and lattice parameters, based on data from Fig. 7. (a) and (b): along (11$\bar{2}$0) direction. (c) and (d): along (10$\bar{1}$0) direction.

stoichiometric value. From t = 32 s to t = 100 s, only very small fluctuations in the RHEED streak spacing is seen, and at t = 100 s, the nitrogen plasma source is turned off.

The same effect is also seen along [10$\bar{1}$0], as the plasma source is being lit. At t = 36 s, N_2 gas is opened into the chamber, at which point the 3× streaks start to fade. At t = 80 s, the plasma source is turned on, and the slope of RHEED spacing gets steeper at this turning point. Similar to [11$\bar{2}$0] direction, at t = 94 s, a total ~3.9% lattice contraction to the GaN stoichiometric value is observed. Similarly, from t = 94 s to t = 150 s, the RHEED streak spacing becomes stable, and only a small fluctuation is found. At t = 150 s, the nitrogen plasma source is turned off, and after that no notable change could be seen in the RHEED streak spacing.

These observations show that nitridation restores the GaN *in-plane* stoichiometric lattice constant which had been modified (increased) by high temperature annealing. Since adding N back to the sample restored the stoichiometric lattice constant, we conclude that high temperature annealing not only removes excess Ga from the surface but also creates N vacancies in the sample which can be re-filled by N plasma exposure. We also observe that additional nitridation does not lead to excess N in the sample, since the *in-plane* lattice constant stabilizes.

As a consequence of these measurements, we therefore find that the incorporation of the Mn δ-doped layer has very little if any effect upon the sample lattice constant, which is however strongly affected by N vacancy concentration. We also measured our sample using XRD and found that GaN stoichiometric *c* values were obtained. This is consistent with our previously reported study of random ~5% Mn-doped GaN, in which no changes to the *c* lattice constant were observed for any growth condition (Ga- or N-rich).[12] This is also consistent with other work which reported negligible lattice constant changes for dilute MnGaN, up to 5% Mn concentration. In most studies of Mn-doped GaN, solubility problems set severe constraints on the maximum Mn concentration, with 5% being considered high.[30] A key advantage of the Mn $\sqrt{3} \times \sqrt{3} - R30^\circ$ structure is setting a well-ordered template for the formation of this high-density δ-doped 2-D layer. Here, we find that even a high 33% δ-doping concentration has no important effect on the surface lattice constant.

It is interesting to note that Cui *et al.* found HM behavior for Mn δ-doping concentrations of both 25% and 50%. In addition, for either case, the magnetic moments per Mn atom were reported to be ~3.8 μ_B. Incidentally, another theoretical paper by Kanoun *et al.*, for Mn bulk doping of *zinc-blende* GaN, reported a very similar value of 4.0 μ_B per cell (3.1 μ_B per Mn) with HM ferromagnetism.[31] The sample reported here, with a Mn content assumed to be ~33% assuming one Mn per $\sqrt{3} \times \sqrt{3} - R30^\circ$ unit cell, therefore represents an intriguing candidate structure for possible magnetic properties (currently under investigation).

D. Overgrowth of monolayers of GaN

Next, the overgrowth of GaN layers on top of the Mn-δ-doped GaN layer is investigated 1 ML at a time. Shown in

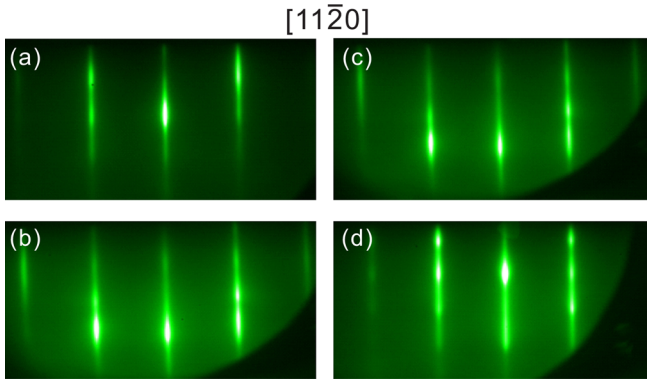

FIG. 9. (a)–(d) RHEED images along (11$\bar{2}$0) direction, corresponding to 1 ML, 3 MLs, 5 MLs, and 11 MLs of GaN overgrowth, respectively.

Fig. 9 is a selection of RHEED patterns corresponding to overgrowth of GaN in such small increments. We see in Fig. 9(a) that after 1 ML of GaN growth, the RHEED pattern remains in a clear and bright 1 × 1. Again, 3 MLs of GaN in total is deposited, and the RHEED pattern is obtained, as shown in Fig. 9(b); a clear and bright 1× pattern is still observed. This process is repeated, and similar results are obtained for GaN overgrowths of 7 MLs [Fig. 9(c)] and 11 MLs [Fig. 9(d)]. Based on the intensity and sharpness of the RHEED patterns, it is evident that GaN overgrows the Mn-covered GaN surface while maintaining crystalline surface order.

The RHEED scan mode image along [11$\bar{2}$0] is taken to record the nitridation and overgrowth of 20 MLs of GaN on top of the Mn/GaN sample [see Fig. 10]. A quantitative

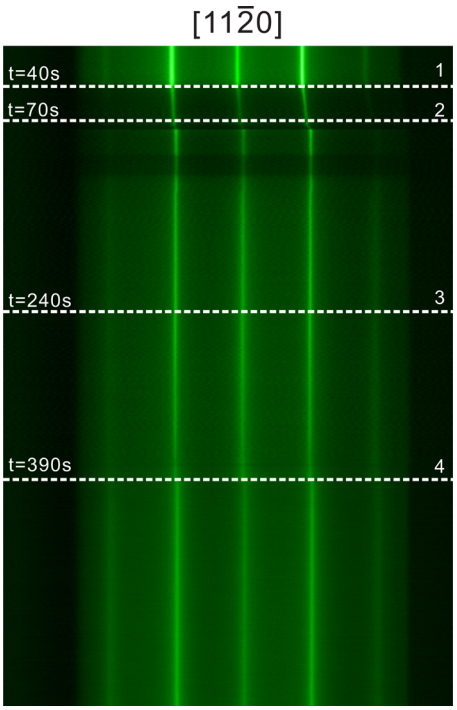

FIG. 10. Scan mode RHEED image along (11$\bar{2}$0) showing effects of nitridation and 20 MLs GaN overgrowth. A total time of 600 s has been recorded. Line 1: t = 40 s, open nitrogen gas. Line 2: t = 70 s, plasma on. Line 3: t = 240 s, open Ga shutter, begin growth. Line 4: t = 390 s, close Ga shutter and turn off N plasma, stop growth.

analysis of the RHEED streak spacing in this process is carefully carried out to clearly identify the lattice constant change involved in this process [see Fig. 11]. At t = 40 s, N_2 gas is filled into the growth chamber at which point the pattern dims as seen in Fig. 10, and as shown in Fig. 11, the RHEED streak spacing starts to increase immediately. At t = 70 s, the plasma source is turned on, and by t = 80 s, a total change of the RHEED streak spacing of 3.3% is found, ending with the GaN stoichiometric lattice constant. Some small fluctuations within ±0.4% of the RHEED streak spacing are seen, once the lattice constant is stabilized.

Gallium nitride overgrowth is then started at t = 240 s, at which point the Ga shutter is opened. Growth of GaN is carried out for 150 s, corresponding to a thickness of ~20 MLs or 50 Å of GaN. The GaN growth region corresponds to a dip in the RHEED streak spacing on the graph. This dip may correspond to the Ga-rich (N-poor) growth condition. At t = 390 s, the GaN growth stops and the sample is cooled down to room temperature. Upon cooling, a slight increase in RHEED streak spacing is seen, corresponding to a small thermal lattice contraction with reducing temperature. Finally, at the end of the total 600 s scan, the lattice constant is very close to that of stoichiometric GaN.

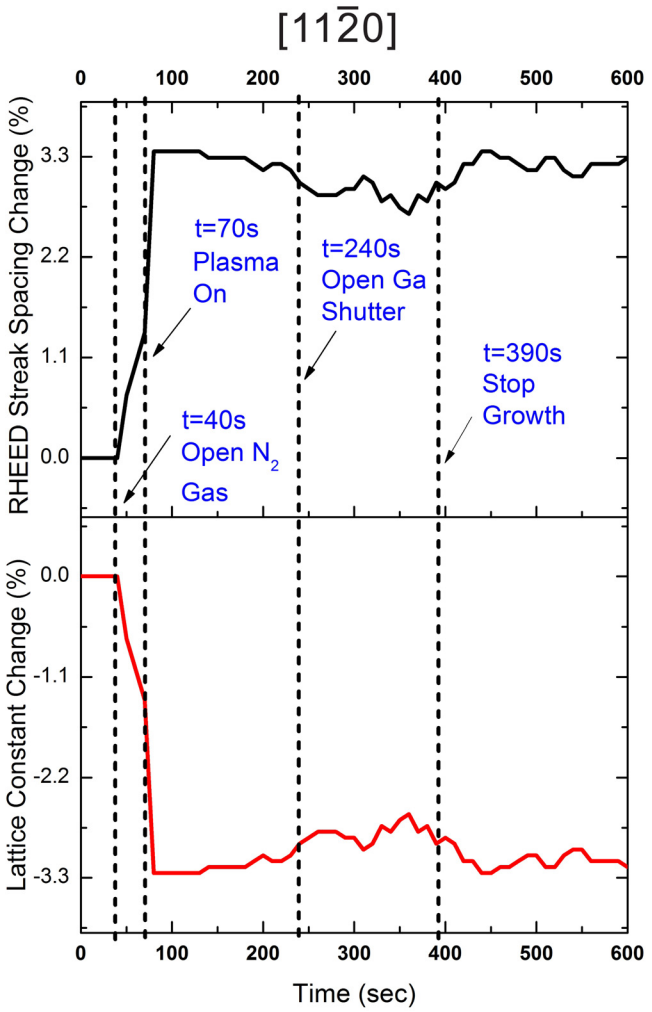

FIG. 11. % changes in RHEED streak spacing and lattice parameter, based on data from Fig. 10. Direction is [11$\bar{2}$0].

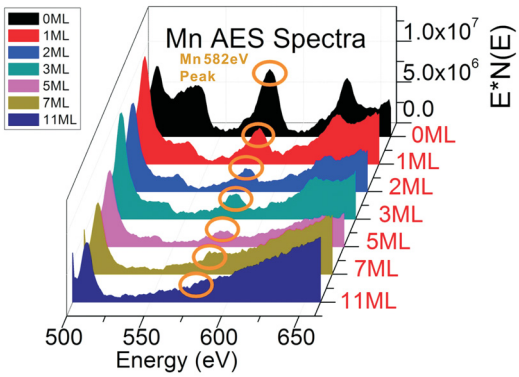

FIG. 12. Mn AES waterfall plot showing decreasing Mn peak intensity with increasing number of GaN MLs.

It is, therefore, found that GaN overgrowth on the Mn δ-doped layer is stable and maintains the GaN stoichiometric lattice constant up to 5 nm in thickness. In fact, we have repeated the experiment and seen that the GaN layer with stoichiometric lattice constant is maintained for much larger thicknesses.

In order to further verify that the Mn remains in the Mn-doped layer, AES spectra were acquired as a function of increasing deposited MLs of GaN (see Fig. 12). In this sequential ML-by-ML experiment, the sample is repeatedly transferred back and forth between the growth chamber and the AES analysis chamber under UHV in order to measure the surface chemical composition after 1, 2, 3, 5, 7, and 11 MLs of GaN. From Fig. 12, we can see that the Mn-specific 582 eV peak is gradually decreasing in height; and that by 11 MLs, the Mn signal is essentially gone. This can be explained as the Mn δ-doped layer being overgrown by the GaN MLs without escaping to the surface of the sample.

Since all AES spectra were recorded with the sample at room temperature, therefore during this experiment, the temperature must be ramped to the growth temperature between every consecutive AES measurement. While this could result in some Mn diffusion away from the interface in principle, the rapid drop off of the Mn signal with increasing GaN MLs

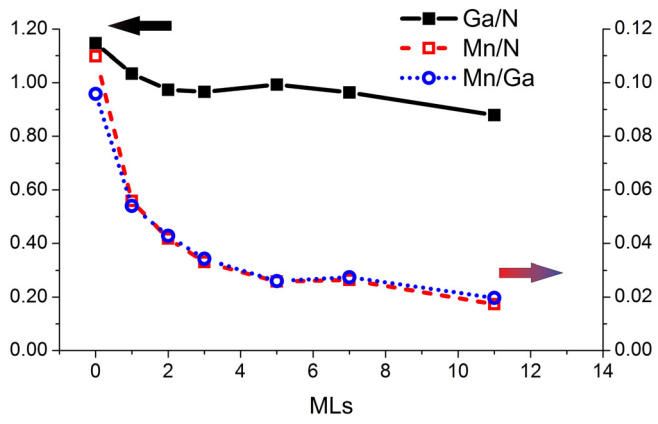

FIG. 13. Surface element concentration ratios carried out by AES analysis. Solid (black) line: Ga/N ratio (left-side scale); dashed (red) line: Mn/N ratio (right-side scale); and dotted (blue line): Mn/Ga ratio (right-side scale).

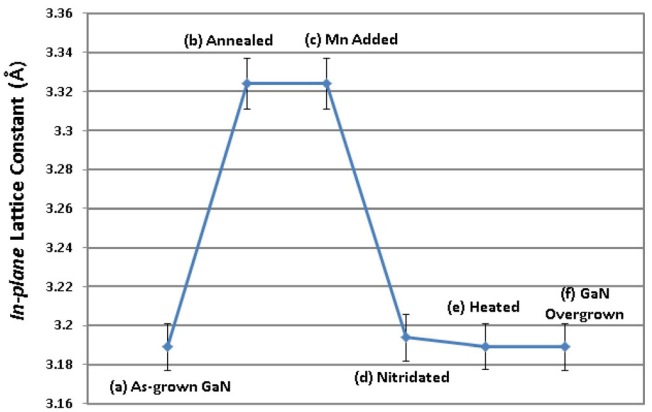

FIG. 14. Evolution of the absolute value of the *in-plane* GaN lattice constant as a function of processing steps including (a) after MBE GaN growth at ~700 °C; (b) after high temperature annealing at 700–750 °C; (c) after addition of Mn to form δ-doped layer; (d) after nitridation; (e) after heating to 700 °C growth temperature; and (f) after GaN overgrowth.

does not support that. This may be due to strong Mn-N-Ga bonding at the interface.

A numerical analysis of the AES data is carried out by computing the Ga/N, Mn/Ga, and Mn/N surface concentration ratios (specifically the AES peak height ratios corrected for sensitivity factors[32]) as a function of increasing MLs of GaN overgrowth. The result is shown in Fig. 13. As can be seen in the figure, the Ga/N ratio (shown in black solid line) gradually decreases, then remains more or less stable with increasing MLs of GaN. The slight downward trend in Ga/N ratio may be due to a slight Ga-poor growth condition.

On the other hand, the Mn/N and Mn/Ga ratios track each other quite closely, both showing a similar trend of exponentially decaying Mn content as GaN is deposited. Such exponentially decaying behavior in concentration ratio for AES data is modeled by two-dimensional overgrowth of layer B (here, GaN) on layer A (here, δ-doped MnGaN).[33] We note that the ratio is not quite zero after 11 MLs, but the result is strong evidence that the Mn δ-doped layer remains intact.

E. In-plane lattice constant evolution

Shown in Fig. 14 is a summary of the evolution of the *in-plane* lattice constant as measured by *in-situ* RHEED, beginning with (a) the MBE-grown GaN substrate, and continuing through the steps of (b) annealing at 700–750 °C; (c) deposition of Mn; (d) nitridation; (e) heating to the growth temperature (~700 °C); and finally (f) GaN overgrowth. The absolute values were calibrated using a metalorganic chemical vapor deposition (MOCVD)-grown GaN substrate, which was introduced into the growth chamber. As can be seen, the as-grown GaN at 700 °C has the stoichiometric value (3.189 Å). The high temperature annealing step results in a rather dramatic lattice expansion by 3%–5% (Note that thermal contraction/expansion over the temperature range of the experiment is maximally ~0.43%, which is within the pixel spacing error of our RHEED measurements ~0.76%). Deposition of Mn does not induce any change in the *in-plane* value. On the other hand, nitridation results in the observed dramatic reduction back to the stoichiometric value (within error bar). Heating to the GaN growth temperature preserves the stoichiometric value (within error bar), and finally overgrowth of GaN continues to maintain the stoichiometric value.

The overall conclusion from this graph is that although high temperature annealing and subsequent nitridation do induce lattice expansion and contraction, respectively, the presence of the Mn δ-doped layer does not have any noticeable effect on the value of the GaN lattice constant. It remains stoichiometric. Therefore, Mn does not appear to induce strain within the structure; this may be an important consideration for future work.

F. Model of Mn δ-layer formation and overgrowth

Presented in Fig. 15 is a proposed model of the Mn δ-layer formation, followed by GaN overgrowth. In the initial step, the Ga adlayer is populated by $\frac{1}{3}$ ML of Mn atoms in substitutional sites, via the $\sqrt{3} \times \sqrt{3} - R30^\circ$ surface reconstruction; at this stage due to our method of high temperature annealing prior to Mn deposition, there also exist some

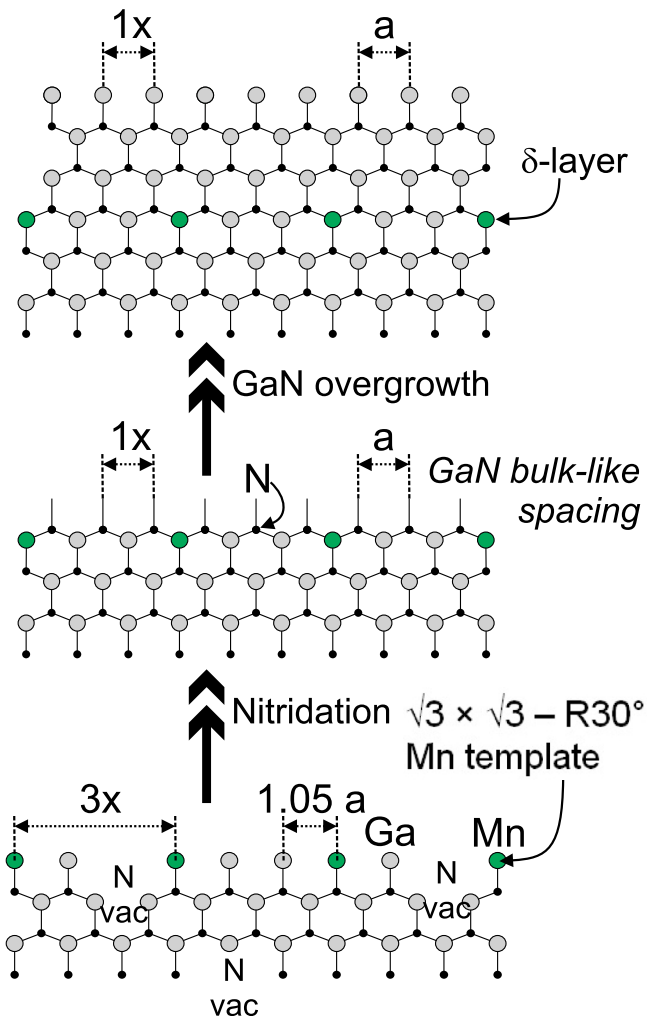

FIG. 15. Model of δ-layer formation and GaN overgrowth, beginning from the Mn $\sqrt{3} \times \sqrt{3} - R30^\circ$ reconstruction template.

N vacancies in the sample. Nitridation of this layer has two important consequences. First, the sample N content is restored, removing N vacancies, bringing the lattice constant back to the GaN stoichiometric value; and second, nitrogen termination of the Mn-containing Ga layer eliminates the 3× RHEED streaks. This nitridated 1×1 MnGaN δ-layer is then ready for GaN overgrowth, which is seen as the final step in the process. The next Ga ML forms bonds with the N atoms, and GaN growth propagates. This model of Mn incorporation is plausible based on the lack of formation of any additional RHEED streaks or spots other than the $\sqrt{3} \times \sqrt{3} - R30^\circ$ streaks, and also because GaN overgrowth proceeds smoothly in a crystalline fashion on the nitridated Mn-containing layer.

IV. CONCLUSIONS

It is shown that Mn δ-doping of wurtzite GaN is achieved by depositing Mn on N-polar GaN$(000\bar{1})$ 1×1, resulting in the formation of a $\sqrt{3} \times \sqrt{3} - R30^\circ$ reconstruction, followed by nitridation. The nitridated Mn δ-doping layer has a stoichiometric GaN-like lattice spacing and is therefore stoichiometric. The nominal concentration of Mn within the Mn δ-doped layer is 33% (assuming one Mn per $\sqrt{3} \times \sqrt{3} - R30^\circ$ unit cell). Overgrowth of GaN on the δ-doped layer maintains crystalline order of the GaN film. The implication is that the Mn is contained within the δ-doped layer with negligible out-diffusion during GaN overgrowth. The successful formation of Mn-δ-doped GaN layers suggests the need for investigations of magnetic properties in order to explore possibilities for developing GaN-based spintronic devices.

ACKNOWLEDGMENTS

Research supported by the U.S. Department of Energy, Office of Basic Energy Sciences, Division of Materials Sciences and Engineering under Award # DE-FG02-06ER46317 (STM studies of nanoscale spintronic nitride systems) and by the National Science Foundation under Award # 0730257 (advancing nanospintronics through international collaboration).

[1]S. A. Wolf, D. D. Awschalom, R. A. Buhrman, J. M. Daughton, S. von Molnar, M. L. Roukes, A. Y. Chtchelkanova, and D. M. Treger, Science **294**, 1488 (2001).
[2]T. Dietl, H. Ohno, F. Matsukura, J. Cibert, and D. Ferrand, Science **287**, 1019 (2000).
[3]S. Krishnamurthy, M. van Schilfgaarde, and N. Newman, Appl. Phys. Lett. **83**, 1761 (2003).
[4]K. Sato, W. Schweika, P. H. Dederichs, and H. Katayama-Yoshida, Phys. Rev. B **70**, 201202 (2004).
[5]K. Sato and H. Katayama-Yoshida, Semicond. Sci. Technol. **17**, 367 (2002).
[6]P. Larson and S. Satpathy, Phys. Rev. B **76**, 245205 (2007).
[7]G. P. Das, B. K. Rao, and P. Jena, Phys. Rev. B **69**, 214422 (2004).
[8]N. Theodoropoulou, A. F. Hebard, M. E. Overberg, C. R. Abernathy, S. J. Pearton, S. N. G. Chu, and R. G. Wilson, Appl. Phys. Lett. **78**, 3475 (2001).
[9]M. L. Reed, N. A. El-Masry, H. H. Stadelmaier, M. K. Ritums, M. J. Reed, C. A. Parker, J. C. Roberts, and S. M. Bedair, Appl. Phys. Lett. **79**, 3473 (2001).
[10]G. T. Thaler, M. E. Overberg, B. Gilla, R. Frazier, C. R. Abernathy, S. J. Pearton, J. S. Lee, S. Y. Lee, Y. d. Park, Z. G. Khim, J. Kim, and F. Ren, Appl. Phys. Lett. **80**, 3964 (2002).
[11]M. E. Overberg, C. R. Abernathy, S. J. Pearton, N. A. Theodoropoulou, K. T. McCarthy, and A. F. Hebard, Appl. Phys. Lett. **79**, 1312 (2001).
[12]M. B. Haider, C. Constantin, H. A. H. Al-Brithen, H. Yang, E. Trifan, D. C. Ingram, A. R. Smith, C. V. Kelly, and Y. Ijiri, J. Appl. Phys. **93**(9), 5274 (2003).
[13]S. Kuroda, E. Bellet-Amalric, R. Giraud, S. Marcet, J. Cibert, and H. Mariette, Appl. Phys. Lett. **83**, 4580 (2003).
[14]M. Bolduc, C. Awo-Affouda, A. Stollenwerk, M. B. Huang, F. G. Ramos, G. Agnello, and V. P. LaBella, Phys. Rev. B **71**, 033302 (2005).
[15]A. P. Li, J. F. Wendelken, J. Shen, L. C. Feldman, J. R. Thompson, and H. H. Weitering, Phys. Rev. B **72**, 195205 (2005).
[16]M. E. Overberg, B. P. Gila, C. R. Abernathy, S. J. Pearton, N. A. Theodoropoulou, K. T. McCarthy, S. B. Arnason, and A. F. Hebard, Appl. Phys. Lett. **79**, 3128 (2001).
[17]N. Theodoropoulou, A. F. Hebard, M. E. Overberg, C. R. Abernathy, S. J. Pearton, S. N. G. Chu, and R. G. Wilson, Phys. Rev. Lett. **89**, 107203 (2002).
[18]V. A. Gubanov, C. Boekema, and C. Y. Fong, Appl. Phys. Lett. **78**, 216 (2001).
[19]A. V. Komarov, A. V. Los, S. M. Ryabchenko, and S. M. Romanenko, J. Appl. Phys. **109**, 083936 (2011).
[20]T. Fukumura, Z. W. Jin, A. Ohtomo, H. Koinuma, and M. Kawasaki, Appl. Phys. Lett. **75**, 3366 (1999).
[21]D. P. Norton, S. J. Pearton, A. F. Hebard, N. Theodoropoulou, L. A. Boatner, and R. G. Wilson, Appl. Phys. Lett. **82**, 239 (2003).
[22]J. S. Lee, J. D. Lim, Z. G. Khim, Y. D. Park, S. J. Pearton, and S. N. G. Chu, J. Appl. Phys. **93**, 4512 (2003).
[23]N. Tandon, G. P. Das, and A. Kshirsagar, J. Phys.: Condensed Matter **18**, 9245 (2006).
[24]S. Dhar, L. Perez, O. Brandt, A. Trampert, K. H. Ploog, J. Keller, and B. Beschoten, Phys. Rev. B **72**, 245203 (2005).
[25]X. Y. Cui, J. E. Medvedeva, B. Delley, A. J. Freeman, and C. Stampfl, Phys. Rev. B **78**, 245317 (2008).
[26]X. Y. Cui, B. Delley, A. J. Freeman, and C. Stampfl, J. Appl. Phys. **106**, 043711 (2009).
[27]A. V. Chinchore, K. Wang, W. Lin, and A. R. Smith, Appl. Phys. Lett. **93**, 181908 (2008).
[28]A. R. Smith, R. M. Feenstra, D. W. Greve, J. Neugebauer, and J. E. Northrup, Phys. Rev. Lett. **79**, 3934 (1997).
[29]A. R. Smith, R. M. Feenstra, D. W. Greve, J. Neugebauer, and J. E. Northrup, Appl. Phys. A **66**, S947 (1998).
[30]M. Kocan, J. Malindretos, M. Roever, J. Zenneck, T. Niermann, D. Mai, M. Bertelli, M. Seibt, and A. Rizzi, Semicond. Sci. Technol. **21**, 1348 (2006).
[31]M. B. Kanoun, S. Goumri-Said, A. E. Merad, and J. Cibert, J. Phys. D.: Appl. Phys. **38**, 1853 (2005).
[32]K. D. Childs, B. A. Carlson, L. A. LaVanier, J. F. Moulder, D. F. Paul, W. F. Stickle, and D. G. Watson, *Handbook of Auger Electron Spectroscopy*, 3rd ed. (Physical Electronics, 1995).
[33]H. Lüth, *Solid Surfaces, Interfaces and Thin Films*, 4th ed. (Springer, 2001), pp. 107–108.